Supplementary Fig. 1 (Li *et al*.)

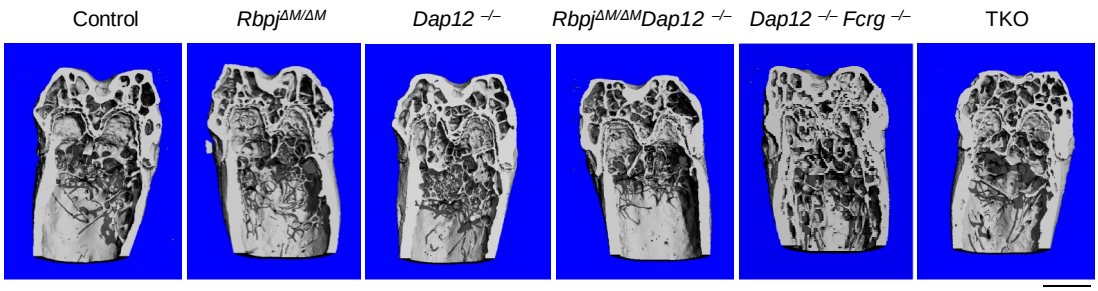

Supplementary Figure 1 Microcomputed tomography (μCT) images of the distal femurs isolated from the indicated bone marrow chimeric mice. "TKO" indicates the *Rbpj*$^{\Delta M/\Delta M}$*Dap12*$^{-/-}$*Fcrg*$^{-/-}$ mice. Scale bar, 1mm.

Supplementary Fig. 2 (Li *et al*.)

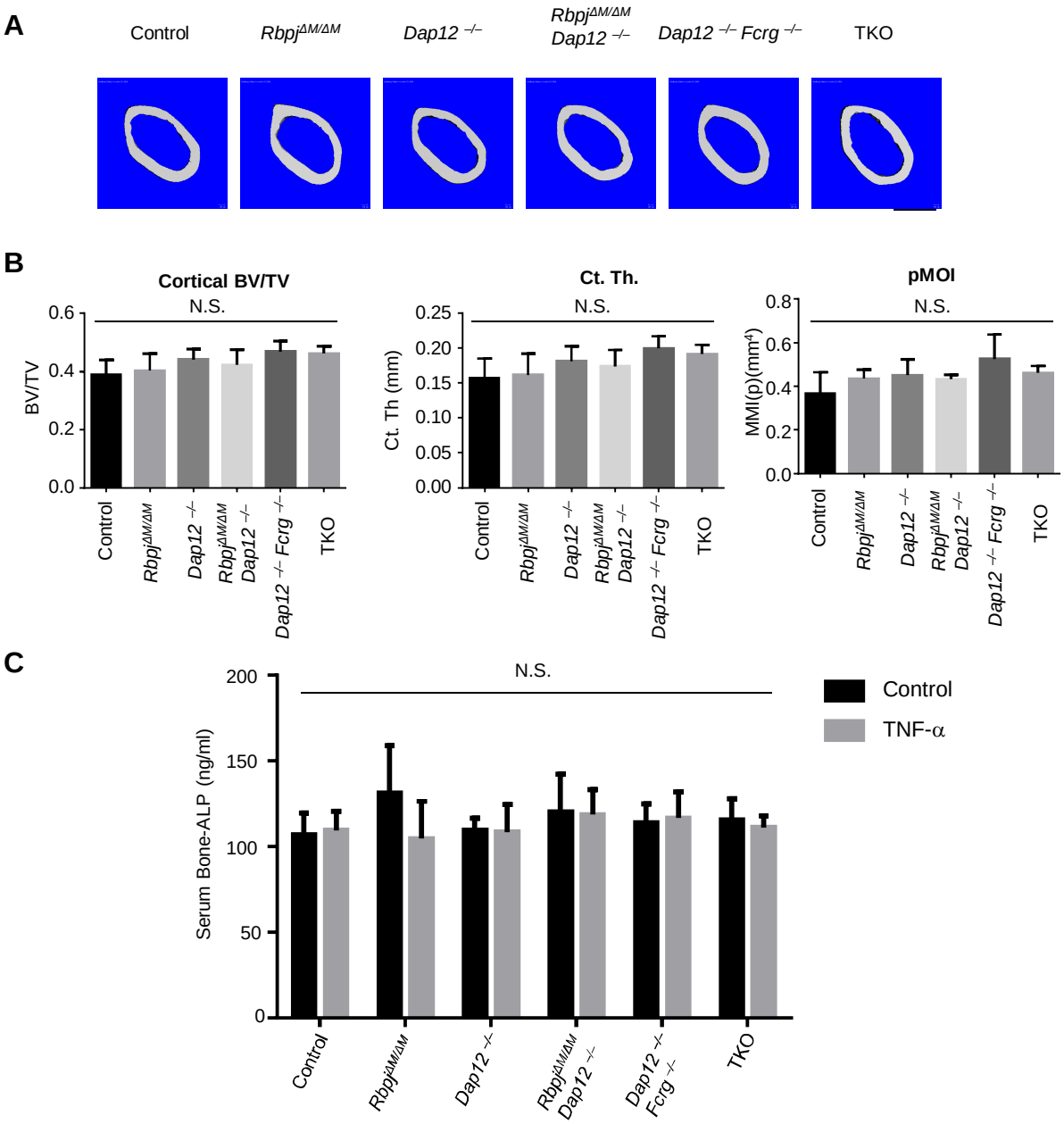

Supplementary Figure 2 RBP-J deficiency does not significantly affect the cortical bone phenotype in the indicated mice. (A) Microcomputed tomography (μCT) images of mid-trunk of the femurs isolated from the indicated bone marrow chimeric mice. "TKO" indicates the *Rbpj*$^{\Delta M/\Delta M}$*Dap12*$^{-/-}$ *Fcrg*$^{-/-}$ mice. Scale bar, 1mm. (B) Cortical bone morphometric analysis of femurs isolated from the chimeric mice. BV/TV, bone volume per tissue volume; Ct Th., Cortical bone Thickness; pMOI, Polar Moment of Inertia; *n* =5 per group. N.S., no statistically significant difference. (C) Concentration of serum Bone-ALP obtained from the indicated mice. *n* = 5 per group. N.S., no statistically significant difference.

Supplementary Fig. 3 (Li *et al*.)

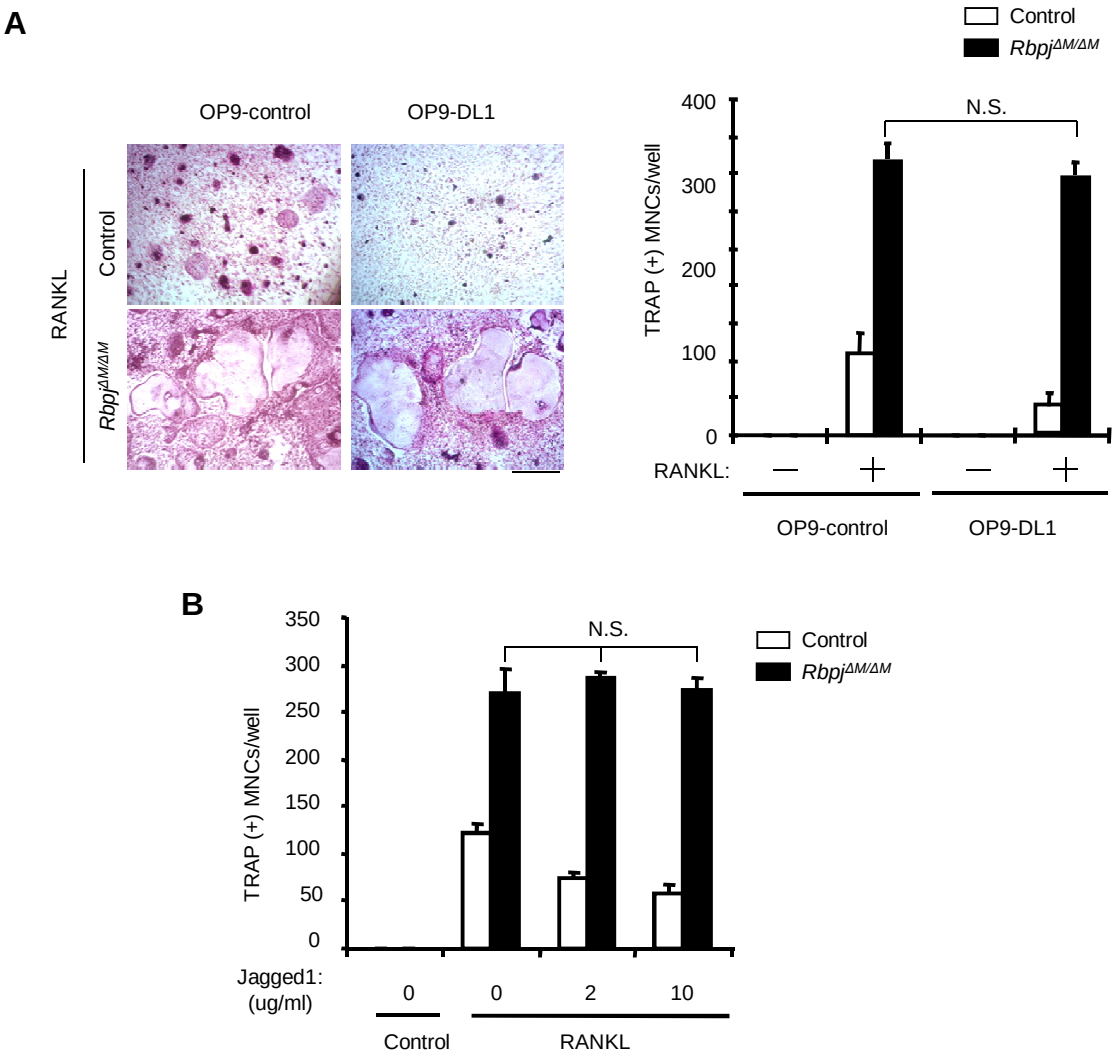

Supplementary Figure 3 Inhibition of osteoclastogenesis by Notch signaling is RBP-J dependent. RBP-J deficiency abolished the inhibition of osteoclastogenesis by Delta-like1 (A) or Jagged1 (B) activated Notch signaling. (A) The control or *Rbpj*$^{\Delta M/\Delta M}$ osteoclast precursors were co-cultured with Delta-like1 overexpressing OP9 cells (OP9-DL1) or the OP9 cells harboring the control vectors (OP9-control) in the present of RANKL for 5 days. Scale bar, 100μm. (B) The control or *Rbpj*$^{\Delta M/\Delta M}$ osteoclast precursors were treated without or with recombinant Jagged1 in the present of RANKL for 5 days. TRAP staining was performed and TRAP(+) MNCs cells were counted. N.S. No statistically significant difference.

Supplementary Fig. 4 (Li *et al*.)

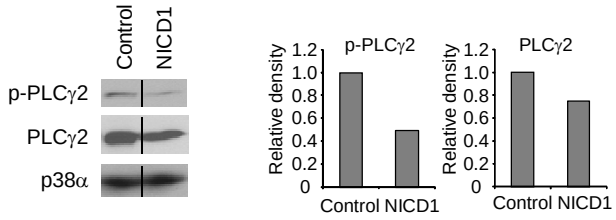

Supplementary Figure 4 Notch-RBP-J signaling suppresses basal PLCγ2 expression. NICD1 overexpression reduced the levels of phospho-PLCγ2 and total PLCγ2. Bone marrow derived macrophages were obtained from the control or *NICD1^{M}* mice (*Rosa^{NICD1};LysMcre* (+)) (ref.29), in which the NICD1 is overexpressed in myeloid cells. The lanes separated by a black line indicate that they were run on the same gel but were noncontiguous. p38α was measured as a loading control. The relative density of the immunoblot bands of phospho-PLCγ2 or total PLCγ2 vs. those of loading control p38α were quantified by densitometry and normalized to the control condition (right panel).

Supplementary Fig. 5 (Li *et al*.)

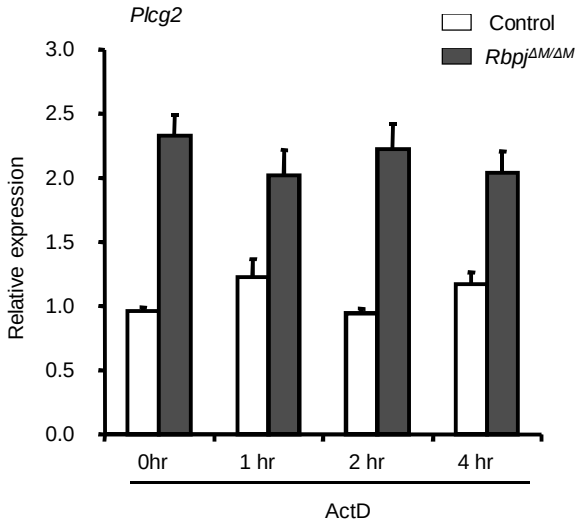

Supplementary Figure 5 mRNA stability of *Plcg2* is not affected by RBP-J deficiency. The control or *Rbpj*$^{\Delta M/\Delta M}$ osteoclast precursors were treated with actinomycin D (5ug/ml) for the indicated times. The mRNA expression level of *Plcg2* was measured by real-time PCR.

Supplementary Fig. 6 (Li *et al*.)

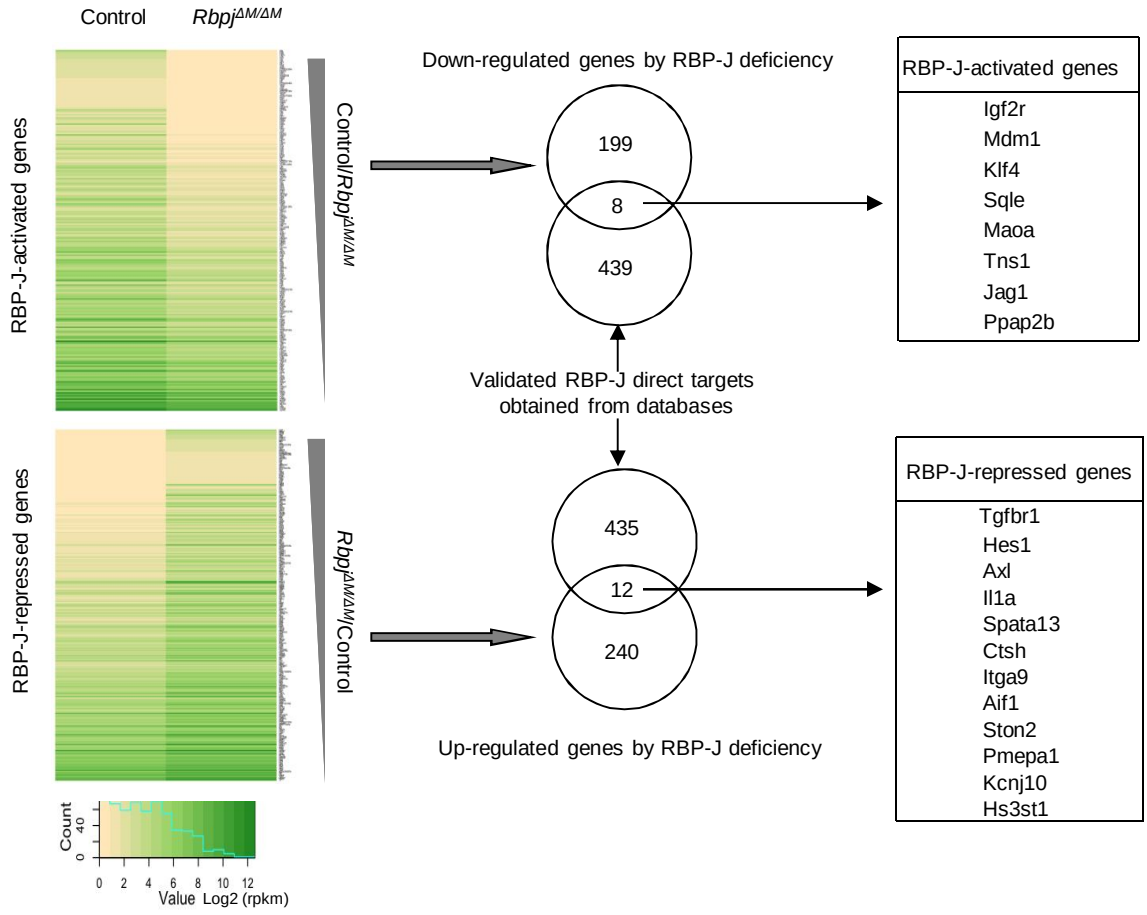

Supplementary Figure 6 Genome wide regulation of gene expression by RBP-J in osteoclast precursors. (Left) RNAseq-based expression heat maps of genes regulated by RBP-J deficiency. The upper panel shows the down-regulated and lower panel represents the up-regulated genes by RBP-J deficiency based on an overlap of two biological replicates of RNAseq experiments using control and *Rbpj*$^{\Delta M/\Delta M}$ osteoclast precursors. Log2 values of RPKMs of a representative RNAseq experiment are shown in the heat map. Genes with log2 ratios between control and *Rbpj*$^{\Delta M/\Delta M}$ cells of more than 1 fold are represented. (Middle) Venn diagrams of the overlap between differentially RBP-J regulated genes (RNAseq) and validated RBP-J direct targets obtained from published databases. (Right) Gene lists of RBP-J putative direct targets in osteoclast precursors.

Supplementary Fig. 7 (Li *et al*.)

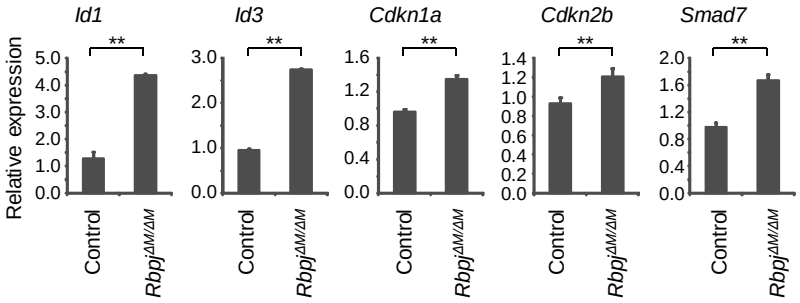

Supplementary Figure 7 RBP-J deficiency enhances cell responsiveness to TGF-β. Quantitative real-time PCR analysis of mRNA expression level of TGF-β responsive genes. Data are representative of at least 3 independent experiments. ***P*<0.01.

Supplementary Fig. 8 (Li *et al*.)

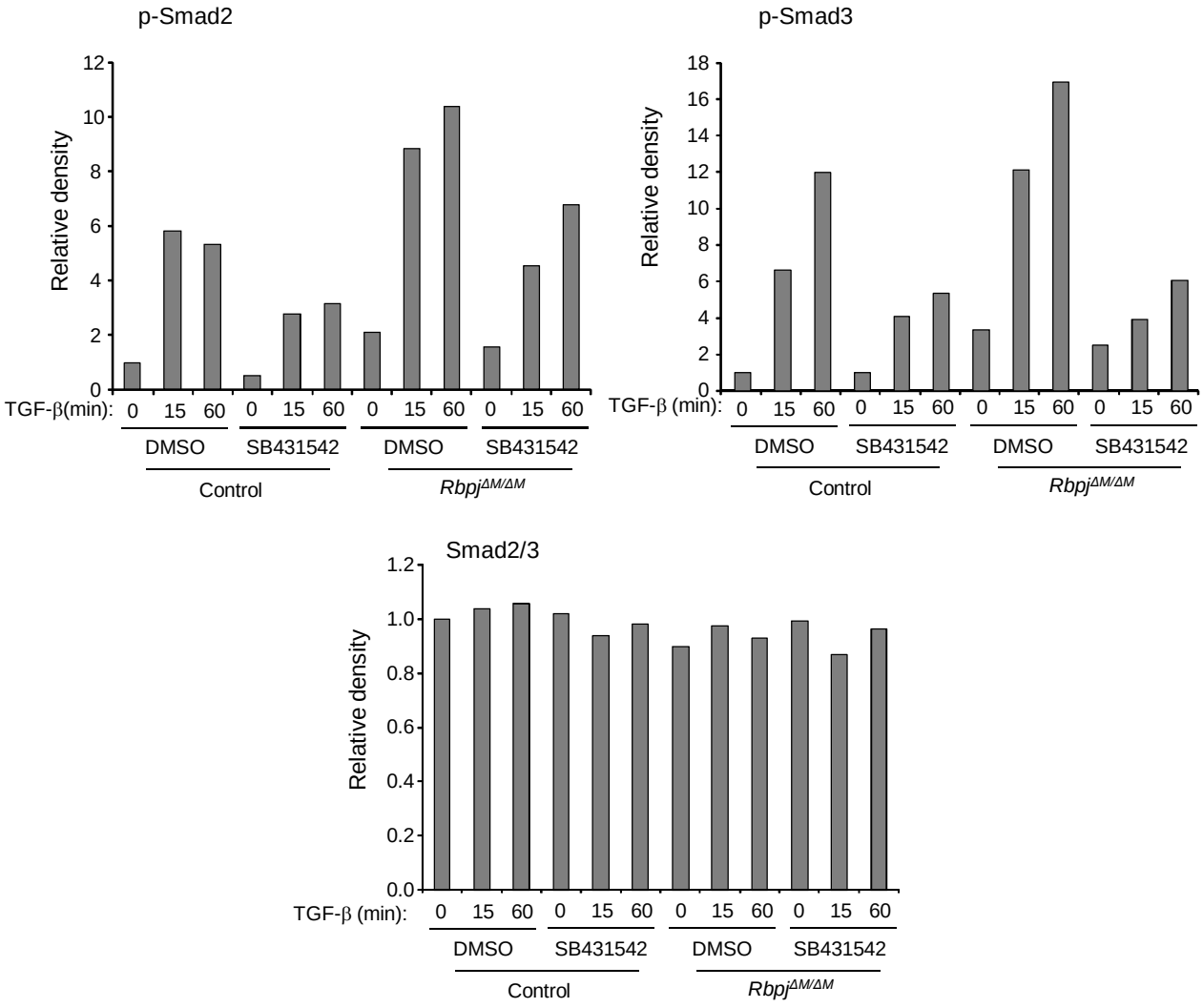

Supplementary Figure 8 The relative density of the immunoblot bands of phospho-Smad2, phospho-Smad3, or total Smad2/3 vs. those of loading control β-tubulin in Figure 5B were quantified by densitometry and normalized to the basal control condition.

Supplementary Fig. 9 (Li *et al*.)

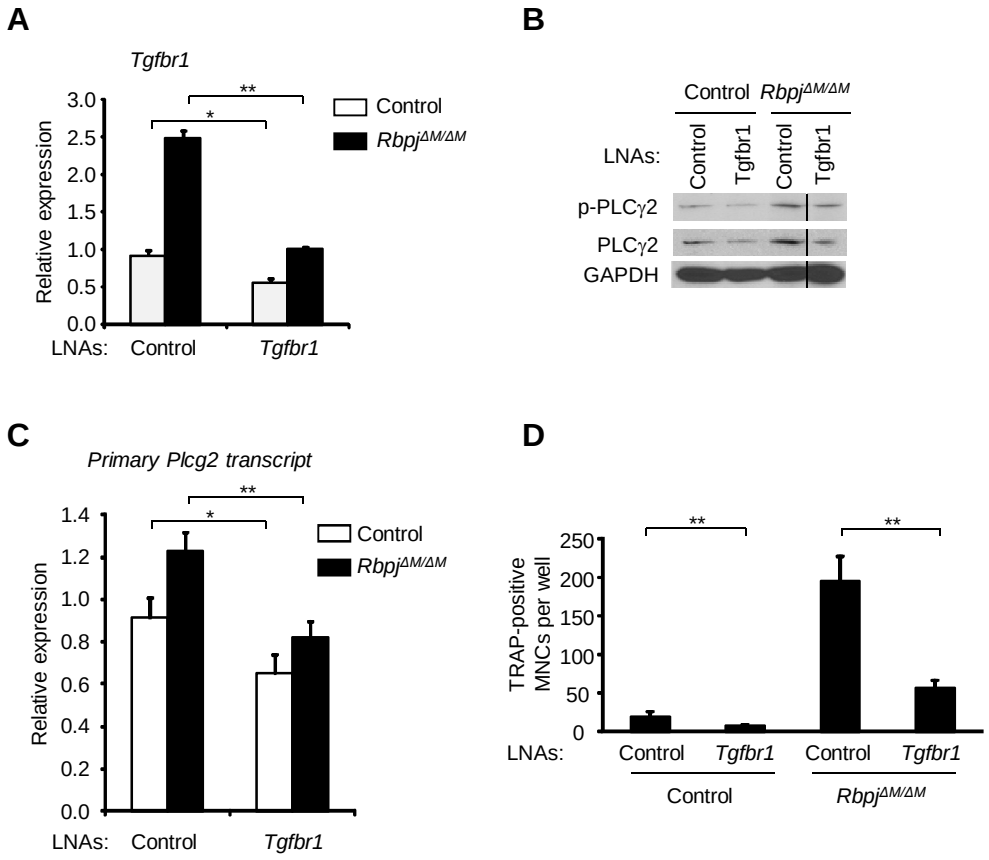

Supplementary Figure 9 RBP-J deficiency suppresses PLCγ2 expression via a TGF-β dependent pathway. (A) Knockdown of *Tgfbr1* in the BMM cells transfected with the indicated LNAs for 24 hours. (B) Immunoblot analysis of phospho-PLCγ2 and total PLCγ2 (The lanes separated by a black line indicate that they were run on the same gel but were noncontiguous), and (C) Primary *Plcg2* transcript expression in BMMs transfected with indicated LNAs for 24 hours. (D) Quantification of TRAP-positive MNCs (>= 3 nuclei per cell) in the culture of BMMs transfected with the indicated LNAs for 24 hours followed by TNF-α treatment for 4 days. **P*<0.05; ***P*<0.01.

Supplementary Fig. 10 (Li *et al*.)

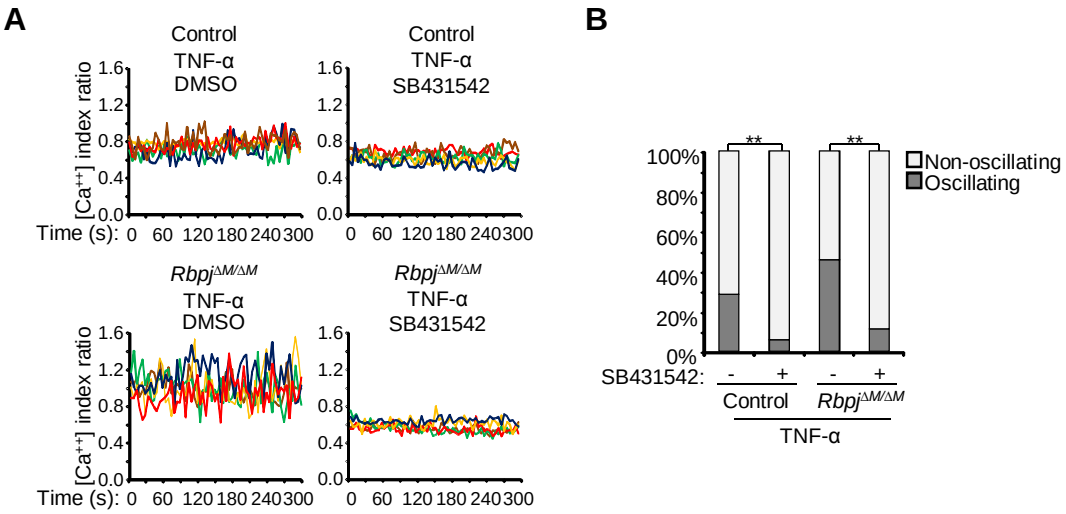

Supplementary Figure 10 Inhibition of TGF-β signaling dampens the TNF-α-enhanced calcium oscillation in the *Rbpj*$^{\Delta M/\Delta M}$ Cells. (A) Representative calcium oscillatory traces of cells treated with TNF-α in the presence of SB431542 (100μM) or DMSO for 24 hours, and oscillating cells were quantified in (B).**P<0.01.

Supplementary Fig. 11 (Li *et al*.)

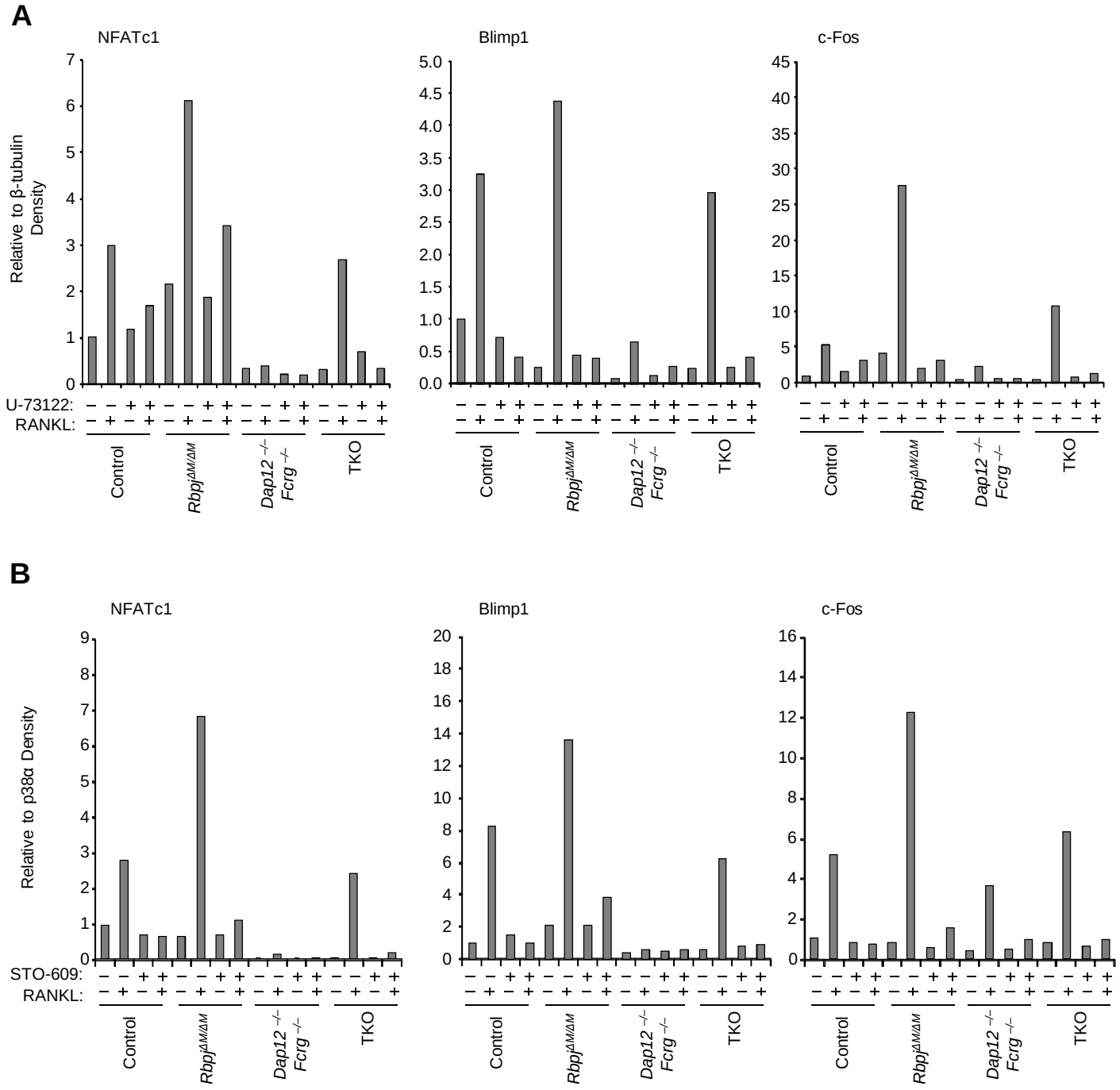

Supplementary Figure 11 The relative density of the immunoblot bands of NFATc1, Blimp1 and c-Fos vs. those of loading control β-tubulin (A, corresponding to Fig. 6A) or p38α (B, corresponding to Fig. 6C) were quantified by densitometry and normalized to each basal control condition.

Supplementary Fig. 12 (Li *et al*.)

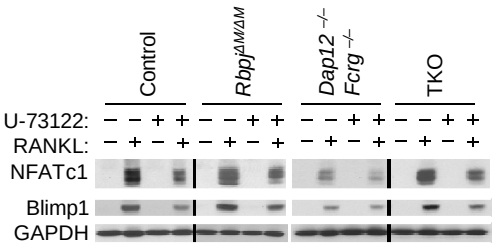

Supplementary Figure 12 Immunoblot analysis of NFATc1expression in the indicated BMM cells treated without or with RANKL for two days. The cells were pretreated for 30 min with PLCγ2 inhibitor U-73122 (10 μM) or its vehicle ethanol that were completely washed away before addition of RANKL. The lanes separated by a black line indicate that they were run on the same gel but were noncontiguous. GAPDH was measured as a loading control.

Supplementary Fig. 13 (Li *et al*.)

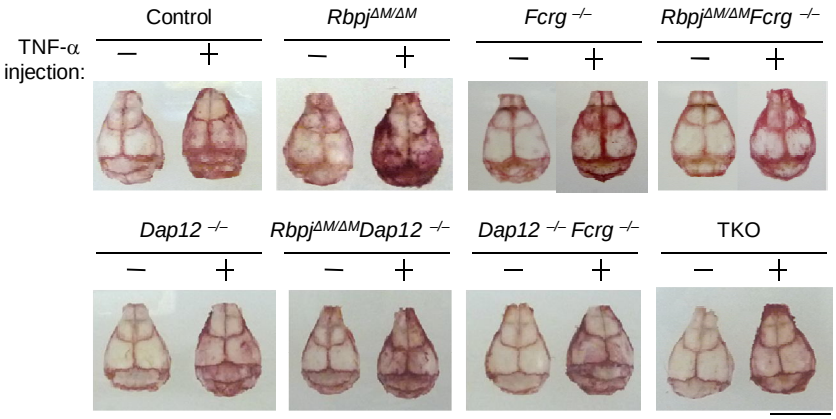

Supplementary Figure 13 TRAP staining of mouse whole calvaria after administration of TNF-α (75 μg/kg body weight) daily to the calvarial periosteum of mice for five consecutive days. Scale bar, 1cm.

Supplementary Fig. 14 (Li *et al*.)

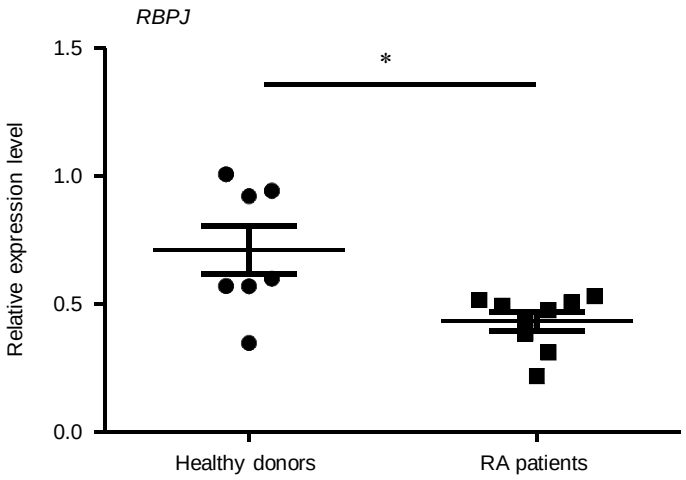

Supplementary Figure 14 The mRNA expression levels of RBP-J are significantly lower in synovial fluid macrophages obtained from 9 rheumatoid arthritis (RA) patients than those in peripheral monocyte derived macrophages from 7 healthy donors. **P*<0.05.

Supplementary Fig. 15 (Li *et al*.)

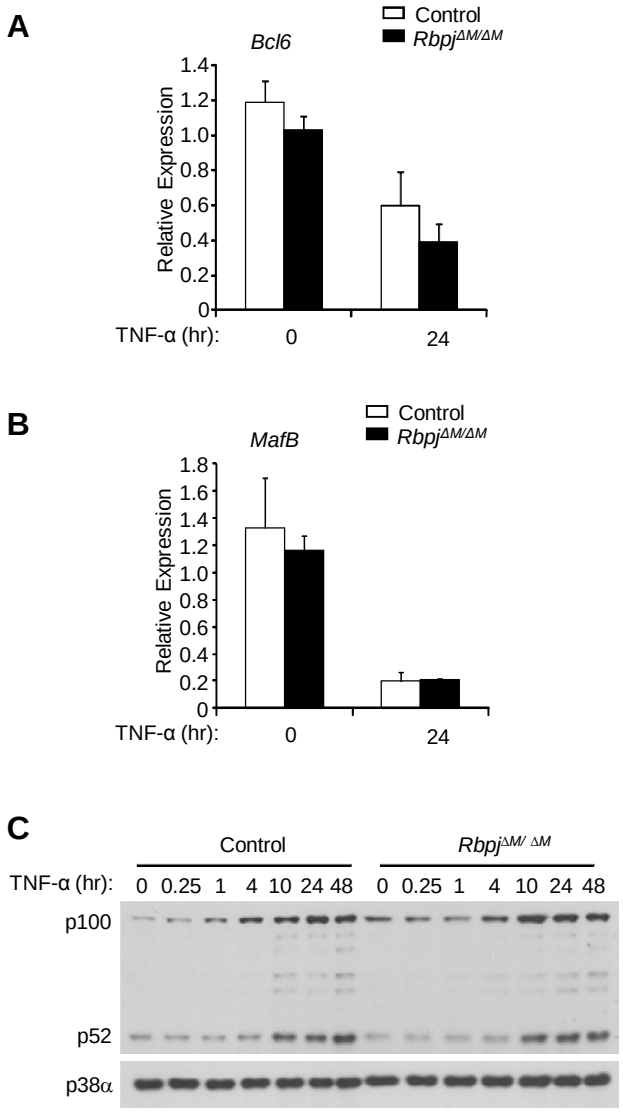

Supplementary Figure 15 Expression of Bcl6, MafB and p100/p52 in response to TNF-α was not affected by RBP-J deficiency. Quantitative real-time PCR analysis of mRNA expression level of Bcl6 (A) and MafB (B). (C) Immunoblot analysis of p100/p52 expression in response to TNF-α at the indicated times. p38α was measured as a loading control.

Supplementary Fig. 16 (Li *et al*.)

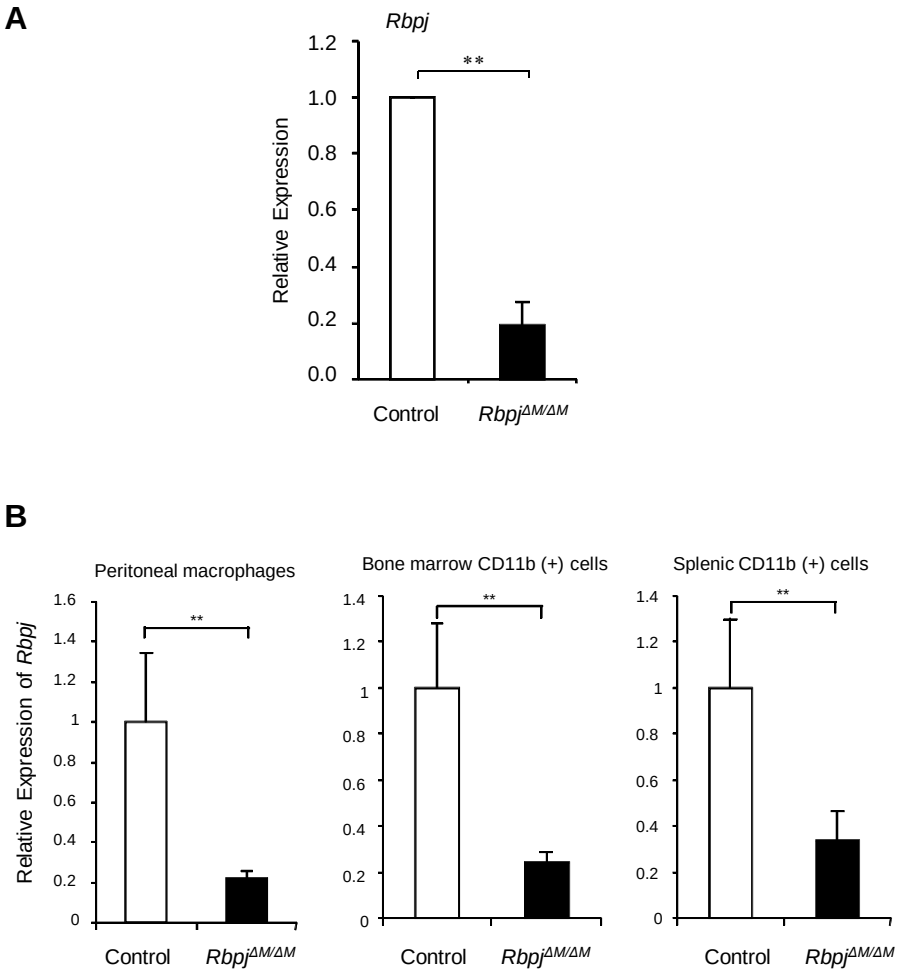

Supplementary Figure 16 The extent of RBP-J deletion efficiency by LysM Cre. (A) The extent of *Rbpj* deletion in bone marrow derived macrophages (BMMs) measured by real-time PCR. n=8 per group. (B) The extent of *Rbpj* in vivo deletion in $Rbpj^{\Delta M/\Delta M}$ mice. Myeloid cells from peritoneum, bone marrow or spleen were obtained by adherence or CD11b magnetic bead selection (Miltenyi Biotec) and RBP-J expression level in these cells was measured by real-time PCR. n=5 per group. $^{**}p<0.01$.